

# Rhenium-Linked Multiporphyrin Assemblies: Synthesis and Properties

Joseph T. Hupp

Department of Chemistry, Northwestern University, 2145 Sheridan Road,  
Evanston, Illinois 60208, USA  
*j-hupp@northwestern.edu*

<b>1</b>	<b>Introduction</b>	145
<b>2</b>	<b>Synthesis of Rhenium-Porphyrin Supramolecular Assemblies</b>	146
2.1	Squares	146
2.2	Rectangles	149
2.3	Planar Dimers	151
<b>3</b>	<b>Porous Materials Based on Supramolecular Assemblies</b>	155
<b>4</b>	<b>Applications and Function</b>	159
4.1	Film- and Membrane-Based Molecular Sieving	159
4.2	Sensing	161
4.3	Catalysis	161
4.4	Fundamental Studies of Energy and Electron Transfer	162
4.5	Light-to-Electrical Energy Conversion	163
	<b>References</b>	164

**Abstract**  $\text{Re}(\text{CO})_5\text{Cl}$  readily reacts with pyridine-derivatized porphyrins to give molecular squares or planar dimers featuring *fac*- $\text{Re}(\text{CO})_3(\text{Cl})$  corners. Chelating ligands, in sequential combination with pyridine-derivatized porphyrins, can be used to obtain related cofacial porphyrin assemblies. Films and membranes displaying molecular-scale porosity can be generated from squares by: (1) van der Waals aggregation, (2) layer-by-layer assembly chemistry based on zirconium-phosphonate links, or (3) polymerization at liquid-liquid interfaces. In addition to molecular sieving, films, membranes, and free assemblies have been used for chemical sensing, oxidative catalysis, and light-to-electrical energy conversion. The assemblies have also been used to investigate fundamental aspects of light-induced energy and electron transfer.

**Keywords** Rhenium · Molecular square · Supramolecular · Porphyrin

## 1 Introduction

Rhenium ions, and especially tricarbonylrhenium(I)chloro fragments, have been used to organize and link pyridine-functionalized porphyrins as molecular squares, rectangles, planar dimers, and more complex structures.

The idea followed from successful syntheses of molecular squares featuring smaller ligand edges such as 4,4'-bipyridine and pyrazine. The attractions of  $\text{Re}(\text{CO})_3\text{Cl}$  in the initial studies were three: (a) *The majority of imine and azine complexes of  $\text{Re}(\text{CO})_3\text{Cl}$  are photo luminescent* [1, 2]. They typically display long excited-state lifetimes, with emission coming from radiative decay of nominally triplet metal-to-ligand charge transfer states. Early on, emission was viewed as a potential signal transduction scheme in host:guest type chemical sensing applications [3]. For ligand-centered emission, such as porphyrin fluorescence, however, the presence of rhenium centers is a detriment. The proximal metals enhance spin-orbit coupling within the photo-excited ligand (the “heavy atom” effect). This accelerates singlet excited state to triplet excited state intersystem crossing, thereby shortening the lifetime of the singlet state, and diminishing the fluorescence yield. (b) *Neutral compounds are readily obtainable*. The single positive charge on rhenium is balanced by a coordinated halide. If neutral ligand edges are used for square construction, the isolated square is charge neutral. Analogous assemblies based on Pt(II) or Pd(II) coordination typically are octa-cationic [4, 5]. Charge neutrality for the rhenium squares eliminates the possibility of channel blocking by counter ions in the solid state. (Often, though, for analogous cationic Pt(II) and Pd(II) assemblies, counter ions have been found to occupy sites between square layers rather than within square cavities, obviating the concern about channel blocking.) Charge neutrality also confers insolubility in water—a potentially useful property if the squares are used as thin-film molecular aggregate materials, as discussed below. Of course, insolubility is a disadvantage if solution-phase applications are envisioned. (c) *Rhenium-imine bonds are inert at ambient temperature*. In contrast, analogous Pt(II) and especially Pd(II) assemblies are somewhat labile, especially if competing ligands are introduced. At elevated temperatures, however, rhenium-imine bonds are labile enough to allow for conversion of kinetic structures (such as open oligomers) to thermodynamic structures during the assembly process. With one exception [6], attempts to use less expensive manganese centers as a substitute for rhenium have been unsuccessful because of the greater lability of Mn(I).

## 2

### Synthesis of Rhenium-Porphyrin Supramolecular Assemblies

#### 2.1

##### Squares

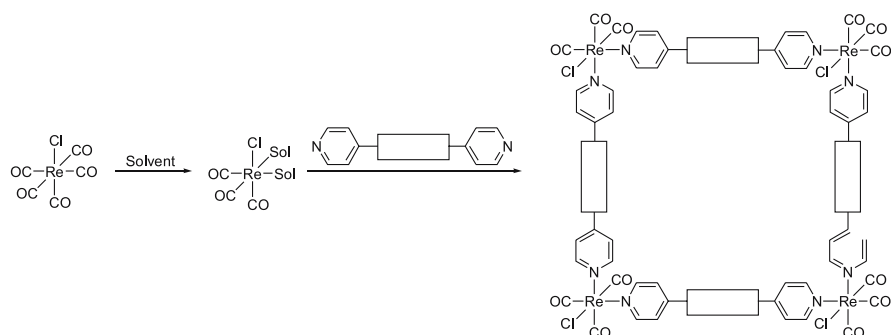
In weakly coordinating solvents such as mixtures of toluene and tetrahydrofuran, the 1 : 1 combination of  $\text{Re}(\text{CO})_5\text{X}$  (X = Cl, Br, or I) and a rigid or semi-rigid dipyriddy ligand generally produces molecular squares in high yield [7–9]. The strong trans labilizing effect of CO allows two of the carbonyl

ligands of  $\text{Re}(\text{CO})_5\text{X}$  to be replaced with solvent molecules. The octahedral geometry of the rhenium coordination sphere ensures that the reactive sites are *cis* to each other. It also ensures that *fac* rather than *mer* compounds are obtained; see Scheme 1.

Subsequent coordination of pyridine-terminated ligands yields complexes defining a roughly  $90^\circ$  pyridine-Re-pyridine angle. With difunctional ligands, the number of Re-imine bonds is maximized by forming cyclic as opposed to open structures. Since the Re-imine bonds are stronger than Re-solvent bonds, cycle formation is enthalpically favored. Strain is minimized by forming structures having square geometries (although triangular assemblies are known [10]).

Contributing to the typically high yields is the generally greater solubility of open structures than squares. Also important is the lability of the Re-imine bond under refluxing conditions in weakly coordinating solvents. Lability allows “mistakes” to be undone, and new bonds to be formed until thermodynamic structures are generated. Note that the halide ligand for each rhenium can be oriented either up or down with respect to the square framework. Four isomers are possible (Fig. 1). While single isomers have occasionally selectively crystallized, the syntheses are believed to produce statistical mixtures of isomers.

The first rhenium porphyrin square to be reported was compound **1**. The square has resisted crystallization, but the structure is supported by FAB mass spectral measurements. From molecular modelling the edge length (rhenium-to-rhenium) is ca. 20 Å. As described below, closely related porphyrinic squares featuring slightly larger cavities have been reported. Characterization of these has proven particularly challenging because of insufficient volatility in high-molecular-weight mass spectrometry experiments. The unique CO infrared signature of *fac*- $\text{Re}(\text{CO})_3(\text{X})\text{L}_2$  species and the relative simplicity of proton NMR spectra for high symmetry cyclic structures enable cycles to be distinguished from acyclic oligomers or polymers, but do



Scheme 1

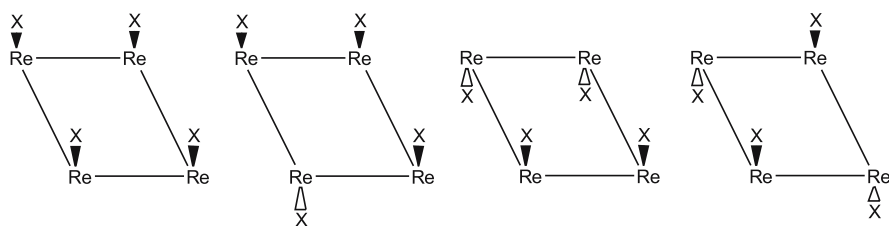
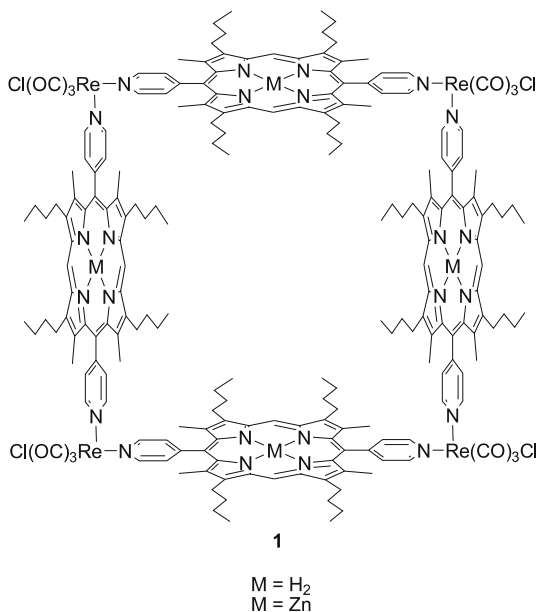


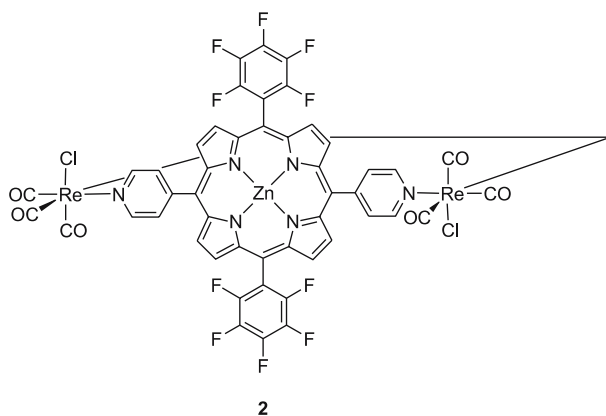
**Fig. 1** Four isomers can be formed for molecules having the formula  $\{\text{Re}(\text{CO})_3(\text{X})(\mu\text{-ligand})\}_4$

not indicate the size of the cycle. In at least one case, vapor phase osmometry has been used to confirm porphyrin square formation [11].

Molecular squares define cavities that are potential hosts for appropriate molecular guests. In methylene chloride as solvent, pyridine binds to the available Zn(II) sites of **1Zn** with an association constant of  $\sim 10^3 \text{ M}^{-1}$ . Whether binding occurs on the square interior or exterior (or a combination of both) has not been established. Recall, however, that Zn porphyrins generally axially bind only one ligand. The free base form of the dipyrindyl porphyrin used to assemble the squares binds to **1Zn** with an equilibrium constant of  $3 \times 10^6 \text{ M}^{-1}$  [7]. The stronger association is a consequence of two-point binding—necessarily occurring within the cavity. Tetrapyrindyl-



**Structure 1**



### Structure 2

porphyrin (TPyP) binds to all four zinc ions, yet is only marginally better associated:  $K_{\text{binding}} = 4 \times 10^7 \text{ M}^{-1}$ . The benefit of additional binding sites is evidently largely offset by the cost of orienting all four porphyrins normal to the plane defined by the rhenium centers. A structural analysis by molecular mechanics and density-functional methods indicated that the porphyrin walls of the lowest energy conformers of the empty square are tilted away from a “vertical” or box-like geometry [12]. A version of the square lacking alkyl substituents but having a pair of pentafluorobenzyl substituents (**2Zn**) was found to bind a representative ligand, 4-phenylpyridine, about an order of magnitude more strongly than does **1Zn** [13]. The stronger binding reflects the electron-withdrawing nature of the perfluorinated substituents and the resulting enhancement of the Lewis acidity of the Zn(II) centers.

## 2.2 Rectangles

Although exceptions exist [14, 15], attempts to prepare tetra-rhenium rectangles simply by combining short and long difunctional ligands with  $\text{Re}(\text{CO})_5(\text{halide})$  have tended to yield mixtures of the corresponding small and large squares instead. An alternative approach is to strengthen the metal-ligand interactions along the short edges of the rectangle by first chelating the rhenium centers to yield either  $\text{Re}_2(\text{CO})_6\text{Cl}_2(\mu\text{-bipyrimidine})$  or  $\text{Re}_2(\text{CO})_8\{\mu\text{-bis}(\text{benzimidazolate})\}$  [16]. Subsequent stoichiometric reaction of the bis(benzimidazolate)-containing edge unit with [5,15-bis(4-ethynylpyridyl)porphyrinato]zinc(II) results in CO displacement and formation of the neutral rectangle **3Zn**. Extraction of chloride ligands with  $\text{Ag}^+$  allows reaction of the bipyrimidine-containing edge with the same porphyrin to give the cationic rectangle **4Zn**. The syntheses were initially attempted using porphyrin 5. The failure to obtain isolable rectangles was attributed

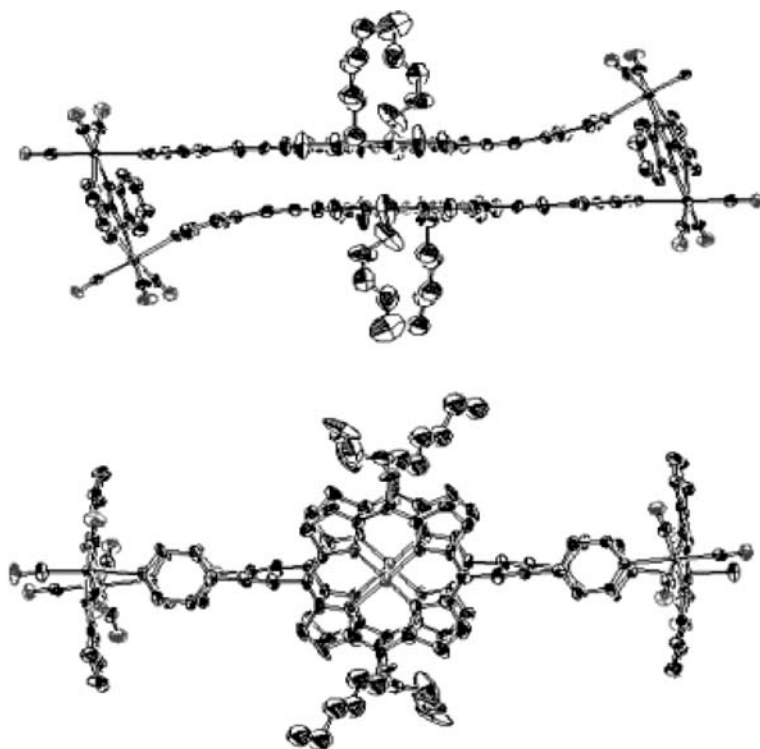
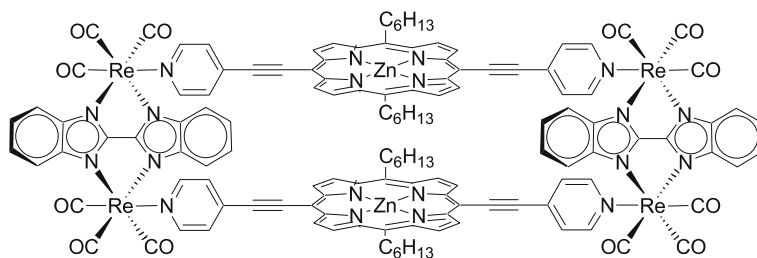


**Fig. 2** ORTEP representations of **3Zn** showing the side view (*top*) and top view (*bottom*) of the co-facial porphyrin systems; hydrogen atoms have been omitted for clarity; the thermal ellipsoids represent 50% occupancy. Adapted from [16]

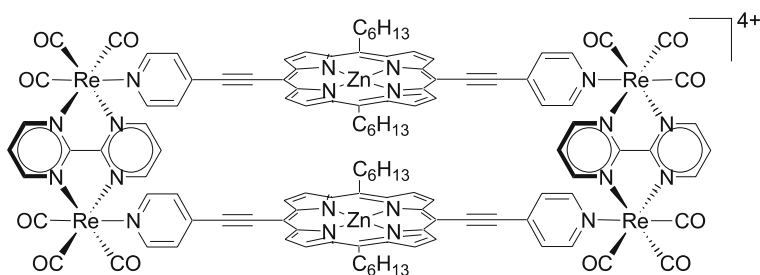


3

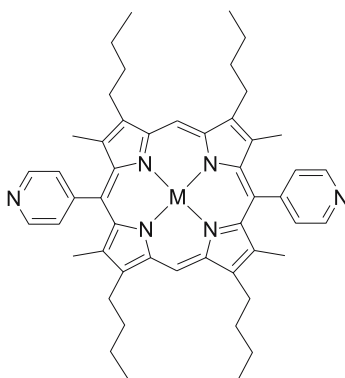
### Structure 3

to unfavorable steric interactions associated with making the pyridine substituents coplanar with the porphyrin.

A crystal structure of **3Zn** showed that cavity collapse occurs—the driving force being van der Waals interactions between the porphyrins; see Fig. 2.



4

**Structure 4**

5

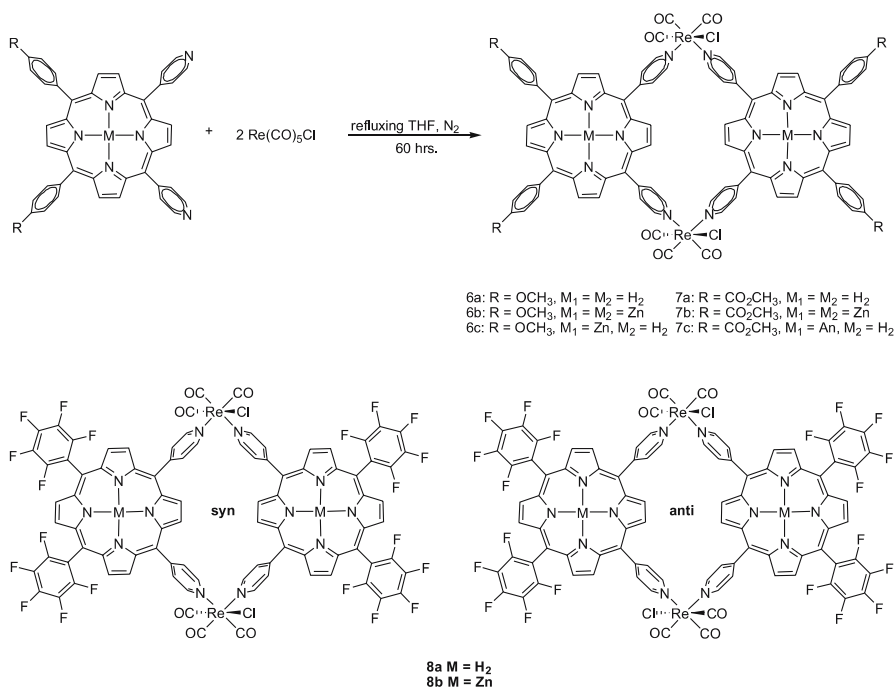
M = H<sub>2</sub>  
M = Zn

**Structure 5**

Consistent with strong van der Waals attraction, attempts to force open the cavity by binding the difunctional ligand 1,4-diazaobicyclo[2.2.2]octane (DABCO), a strong Lewis base, to the available pair of zinc ions were not successful.

**2.3****Planar Dimers**

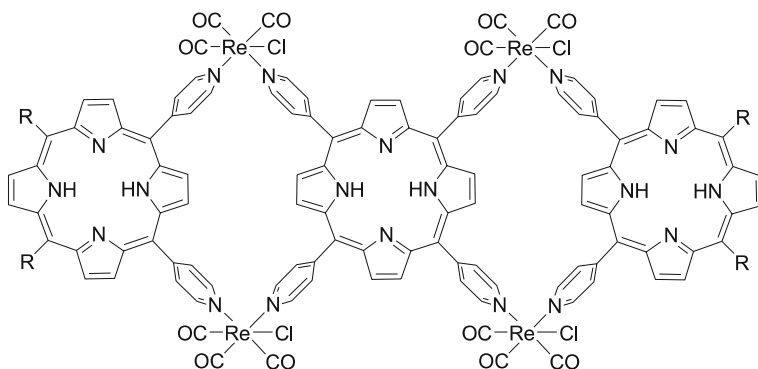
The strong preference for *cis* substitution of pentacarbonyl halo rhenium(I) synthons has been exploited to prepare dimers and hetero dimers of 5,10-pyridyl derivatized porphyrins; see compounds 6–8 and Scheme 2 [13, 17]. Related chemistry has been demonstrated with platinum(II) and palladium(II) compounds where square planar coordination is used to an advantage [18]. In contrast to the square planar compounds, the octahedral



### Scheme 2

coordination of rhenium yields distinct syn and anti isomers with respect to halide ligand configuration. (For simplicity, only one of the compounds has been sketched in both syn and anti form. Higher symmetry octahedrally coordinated Ru(II) compounds, lacking the complications of isomer formation, have also been reported [19] and are discussed elsewhere in this volume.) The isomers display identical <sup>1</sup>H NMR spectra, absorption spectra and fluorescence spectra, but they are separable via chromatography on alumina. To assign the configurations of separated isomers an interesting photophysical approach, transient direct-current photoconductivity, was used. This technique reports on changes in dipole moment,  $\mu$ , upon photoexcitation. More precisely, it measures the quantity:  $\mu^2$  (ground state) –  $\mu^2$  (excited state). The ground-state dipole moment for the anti isomer is zero by symmetry, but greater than zero for the cis isomer. Photo excitation causes identical changes in dipole moment ( $\mu$  (ground state) –  $\mu$  (excited state)) for the two isomers, but different changes in  $\mu^2$  (ground state) –  $\mu^2$  (excited state).

A useful extension (not yet reported) would be to replace the halide ligands with larger functional ligands (other chromophores, energy or electron accepting units, receptors for molecular guests, etc.). Another potentially attractive extension (not yet reported) would be incorporation of tetrapyrridyl

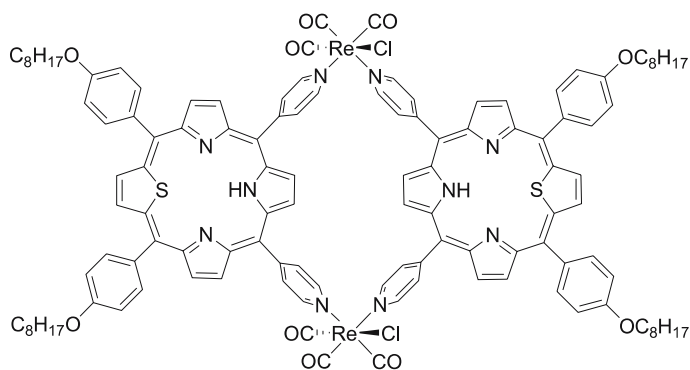


9

**Structure 6**

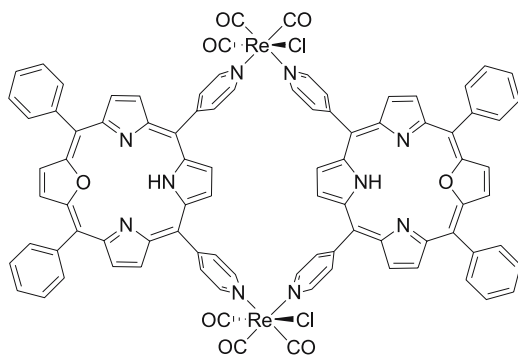
porphyrin repeat units as suggested in structure 9. An extension that has been reported is dimer and hetero dimer formation from sulfur and oxygen substituted porphyrins; see compounds 10–12 [20].

In the presence of 4,4'-bipyridine, the zinc metallated dimers **6b** and **8b** form ligand-pillared cofacial pairs of dimers, **6d** and **8c**; see Scheme 3 [13]. These assemblies are highly reminiscent of the ruthenium-linked tetraporphyrinic assemblies of Iengo and coworkers [21]. These assemblies, like the ruthenium ones, are formed in an “all or nothing” fashion, as evidenced by the lack of intermediate species in titrations of the dimers with the pillars. In other words, the assembly process is a cooperative one: the binding constant for the second pillar is significantly larger than the first. The cooperative behavior is a consequence of the pre-organization achieved by the receptors

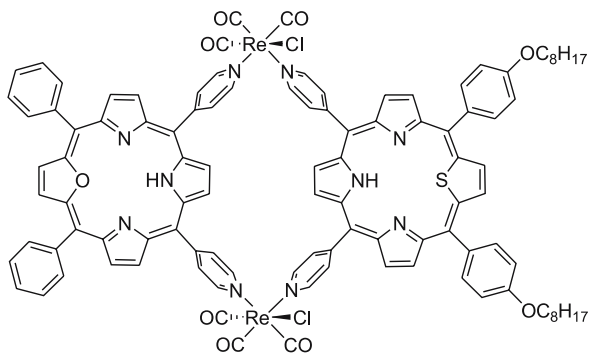


10

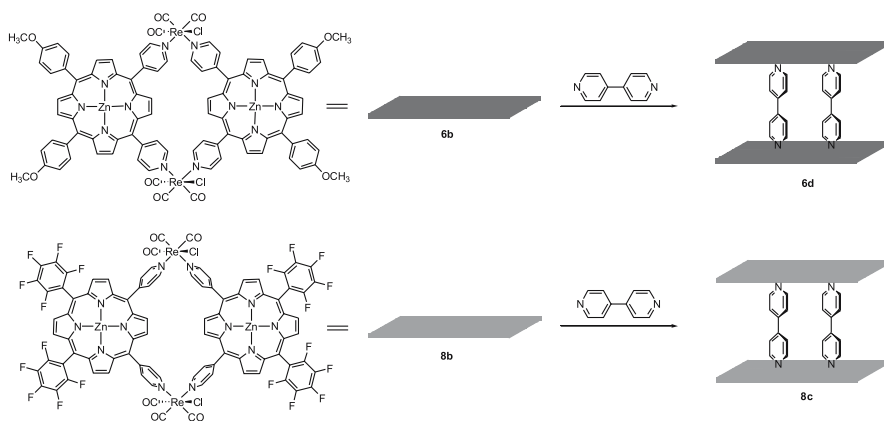
**Structure 7**



11

**Structure 8**

12

**Structure 9****Scheme 3**

once the first pillar is in place. An indication of the degree of cooperativity in binding was provided by comparative studies with the monofunctional ligand, 4-phenyl-pyridine. To account for differences in stoichiometry, values of  $c_{50}$ —the concentration where half the assemblies are dissociated—were determined. The values were about 20-fold lower for **8c** than for the 4-phenyl-pyridine assembly. They were about 4-fold lower for **6d** than for **8c**, consistent with the greater Zn(II) Lewis acidity for the pentafluorophenyl-derivatized dimer.

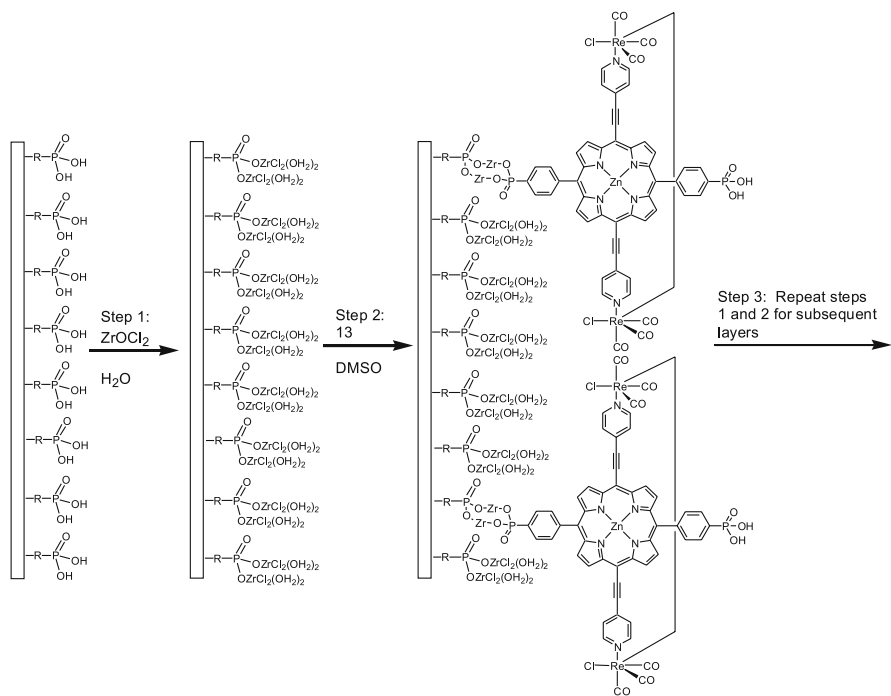
### 3

#### Porous Materials Based on Supramolecular Assemblies

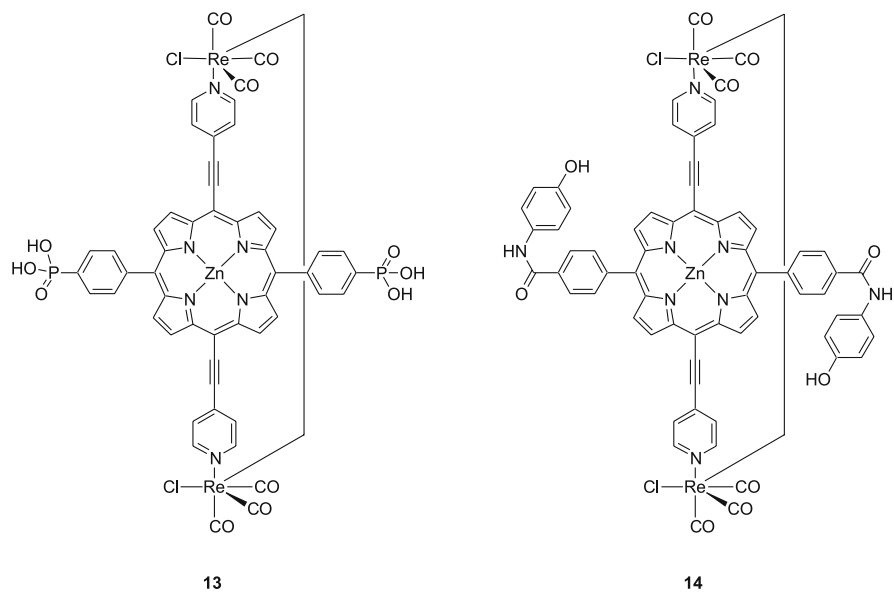
Several studies have described the behavior of thin films of molecular square **1** (see Sect. 4). The films consist simply of molecular aggregates where advantage is taken of the insolubility of the squares in water, in particular, to retain the molecules as functional films. Careful evaporative casting from solvents such as chloroform was found to yield essentially pinhole-free films, in some cases with average film thicknesses as low as  $\sim 25$  nm [22]. Useful films have been prepared on glassy carbon, indium-tin oxide, glass, and mesoporous polyester membranes. Modification of the thin-film materials by Zn(II) ligation of various imines and other nitrogen donors was demonstrated [23]. Interestingly, binding proved to be much more persistent in the film environment than in solution (based on comparisons to soluble porphyrins).

More robust films have been obtained by using the phosphonate-functionalized square, **13Zn**, and employing a layer-by-layer assembly scheme [24]. This scheme, which builds on work by several research groups, exploits the high affinity of phosphonates for Zr(IV) [25, 26]. Film growth can be initiated either by direct attachment of the octa-phosphonated square to a metal-oxide surface or by first derivatizing the supporting surface with a zirconium binding ligand. Note that two steps are entailed in addition of each layer (Scheme 4).

This ensures that only one layer is added per assembly cycle, so allows for very good control over film thickness. This point is illustrated in Fig. 3 where film thicknesses, measured by atomic force microscopy, are plotted against the number of assembly cycles. From the figure, the average layer thickness is ca. 1.8 nm, compared with an expected thickness of 2.5 nm if the walls of the square are strictly vertical. That the observed value is smaller suggests that the squares are configured in a partially collapsed form. Film characterization by X-ray reflectivity, X-ray fluorescence, and long-period X-ray standing wave measurements corroborate the partial collapse, or tilting of the walls, of film-confined squares [27]. The measurements also indicate that appreciably more zirconium is incorporated than implied by Scheme 4.



Scheme 4



Structure 10

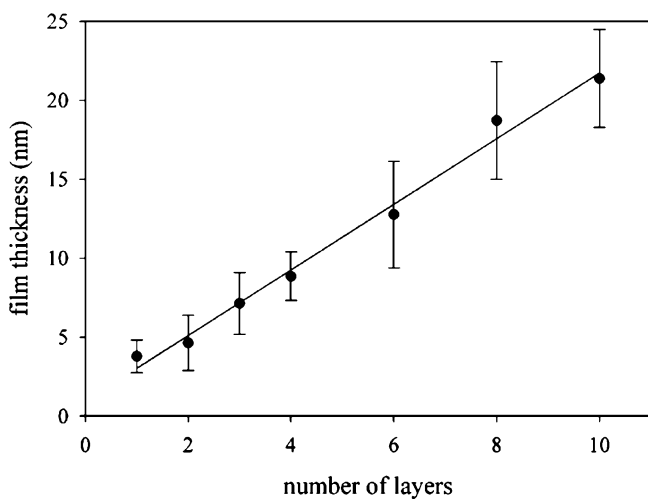
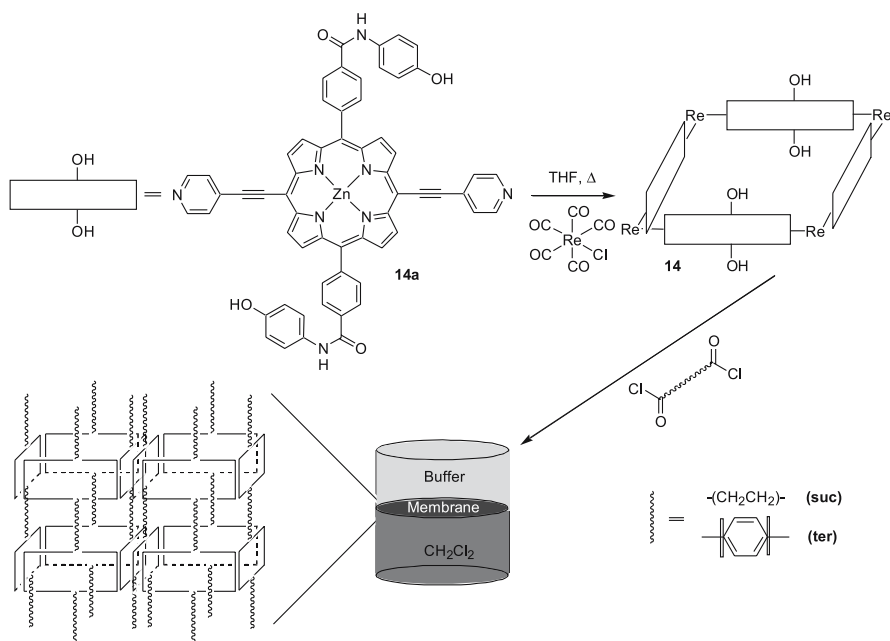


**Fig. 3** AFM heights for ZrP films of 13 assembled on glass. Adapted from [24]



**Scheme 5** Synthesis and interfacial polymerization of molecular square 14. For the interfacial polymerization, the square is confined to the aqueous phase and the acid chloride linker to the organic phase. The polymer structure shown is idealized for illustrative purposes; the actual structure lacks net monomer orientation and is almost certainly cross-linked

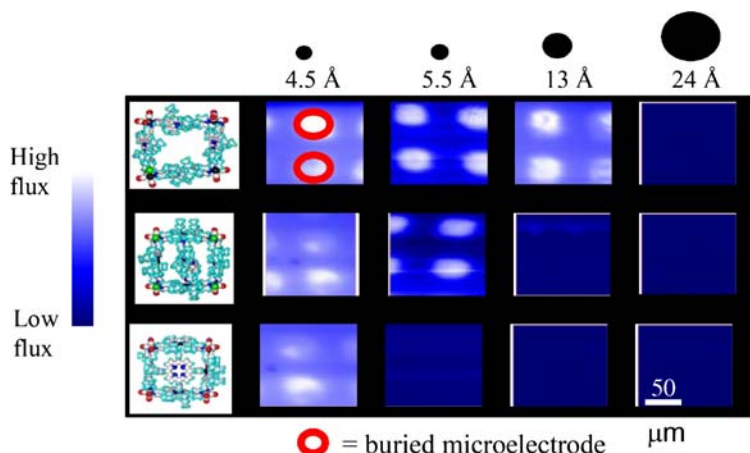


**Fig. 4** Scanning electrochemical microscopy images of  $200\ \mu\text{m} \times 200\ \mu\text{m}$  areas on micropatterned conductive glass slides: the columns (*from left to right*) correspond to electrode areas featuring a thin-film overlay of open or cavity-modified squares. The rows correspond to the following redox mediators: (A) 2 mM ferrocene-methanol (diameter  $\sim 4.5\ \text{\AA}$ ); (B) 3 mM  $\text{Ru}(\text{NH}_3)_6^{3+}$  (diameter  $\sim 5.5\ \text{\AA}$ ); (C) 5 mM  $\text{Fe}(1,10\text{-phenanthroline})_3^{2+}$  (diameter  $\sim 13\ \text{\AA}$ )  $E_{\text{plat}} = 1.0\ \text{V}$ ,  $i = 3.5\ \text{nA}$ ; and (D) 10 mM  $\text{Fe}(4,7\text{-phenylsulfonate-}1,10\text{-phenanthroline})_3^{4-}$  (diameter  $\sim 24\ \text{\AA}$ ). All solutions contained 0.1 M  $\text{KNO}_3$  electrolyte. Adapted from [22]

The layer-by-layer assembly approach also allows defects or pinholes to be overwritten. Electrochemical measurements indicated that detectable pinholes are typically eliminated once three layers are formed [24].

A limitation of the layer-by-layer assembly method is that the resulting films must be supported by a rigid platform. An alternative approach that enables free-standing films (membranes) to be fabricated is polymerization at liquid/liquid interfaces. Porphyrin squares featuring reactive phenolic substituents (**14Zn**) were dissolved in buffered water and allowed to react with small bis(acid chloride) cross-linkers present in a water-immiscible chloroform phase (see Scheme 5) [28]. Condensation yields ester linkages and a thin porous polymeric film. Closely related nonporous film formation chemistry has been described by Wamser and coworkers based on appropriately functionalized pairs of monomeric porphyrin reactants [29]. Because film formation at the liquid/liquid interface inhibits reactant transport, the polymerization process is self-limiting (Fig. 4). Additionally, because the reactant flux is highest at defect sites in the membrane, pinholes are automatically filled. The thicknesses of harvestable films ranged from about 300 to 2500 nm.

## 4 Applications and Function

### 4.1 Film- and Membrane-Based Molecular Sieving

Simple molecular-aggregate type films have proven surprisingly effective as molecular sieves. In one study involving films of **1** cast on mesoporous polyester membrane supports, molecular transport was examined using a U-tube configuration, with the membrane as the size-selective barrier between solutions [30]. Transport was observed via UV-vis absorption by the permeant in the receiving solution. Films were found to be permeable to phenol and to a 13-Å diameter probe, but blocking toward a 24-Å diameter probe. No dependence on molecular charge was seen. The findings are consistent with an estimated 18-Å diameter for the square cavity. In an additional study, the square cavity was bisected by binding a fifth dipyrridyl porphyrin to two of the four available Zn(II) sites of **1Zn**. These cavity-modified films proved permeable to phenol but blocking toward the 13-Å probe. Synchrotron X-ray studies showed the films to be amorphous. Cross-sectional microscopy studies indicated film thickness of ca. 16 μm plus another 9 μm of porphyrinic material infiltrating the support pores.

Vapor permeation of membrane-supported films of **1Zn** has also been studied [31]. Examined as permeants were benzene, toluene, 4-picoline, 2-picoline, cyclohexane, and methylcyclohexane. In pair-wise comparisons modest permeation selectivities were observed (i.e., factors of 1.1 to 9, depending on the permeant pairs compared). The competitive transport measurements were made at equal vapor pressures for the component pairs. The selectivities decrease if comparisons are made at equal reduced vapor pressures,  $P/P_0$ , where  $P_0$  is the vapor pressure at saturation. Nonspecific sorption of volatile compounds at a given partial pressure generally inversely correlates with values for the saturated vapor pressure.

Scanning electrochemical microscopy was used to examine molecular transport through the same material, but now on a conductive platform. Water-soluble redox probe molecules of various sizes were used, with electrochemical signals being observed only from those small enough to permeate the film. Figure 4 shows how the size cutoff changes as the cavity size is altered by incorporating either a dipyrridyl- or tetra-pyrridyl porphyrin guest.

Similar measurements using either walljet electrochemistry or steady-state microelectrode voltammetry have been reported for layer-by-layer assembled and interfacially polymerized materials, respectively [24, 28]. Additional measurements were made spectrophotometrically with polymerized porphyrin squares by using a U-tube. Results summarized in Fig. 5 revealed the following: (a) After normalizing for differences in film thickness, transport through polymeric membranes is two to three orders of magnitude faster

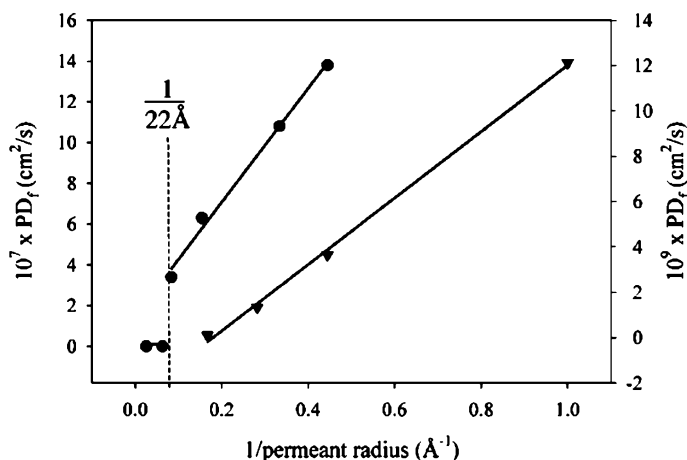


**Fig. 5**  $PD_f$  values for ZrP-assembled (*right axis*) and interfacially polymerized (*left axis*) films of porphyrinic molecular squares **13Zn** (▼) and **14Zn** (●), respectively, as a function of the inverse radius of the permeant. ( $PD_f$  = permeability = (solution-to-film partition coefficient)  $\times$  (film-based diffusion coefficient)). Adapted from [24]

than through layer-by-layer assembled films. (b) A sharp size cutoff exists for the polymeric materials, but layer-by-layer assembled films show a gradual cutoff. (c) For the polymeric material the size cutoff agrees well with the

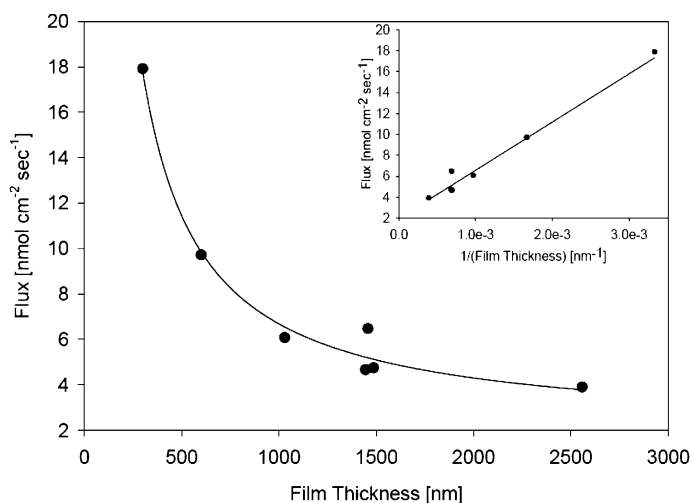


**Fig. 6** Probe molecule flux as a function of film thickness for an interfacially polymerized film derived from molecular square **14Zn** and succinyl chloride. The *line* is drawn to show a first order inverse fit to the data. (*Inset* shows linearity of the reciprocal plot.) Adapted from [28]

cavity size for an isolated square. For layer-by-layer assembled materials it appears to be smaller. These differences have been ascribed to swelling and flexing of the polymeric material versus rigidity for the zirconium phosphonate linked films.

Shown in Fig. 6 is the dependence of molecular flux on polymer film thickness. The observed inverse correlation is characteristic of permeation-controlled transport. In other words, fluxes are limited by rates of diffusion through the film rather than partitioning from the solution to the film. Similar behavior has been observed for molecular aggregate films.

## 4.2

### Sensing

A brief report showed that molecular square **1Zn** could be used to detect binding of sodium and potassium cations by a crown ether featuring a pendant pyridine [32]. The crown ether ligand was observed to bind via the pendant pyridine to the available Zn(II) sites of the porphyrin square. Accompanying the binding was a decrease in fluorescence intensity that was reversed upon capture of an alkali metal cation by the crown.

Micropatterned porous films of molecular square **1Zn** were observed to diffract visible light. Uptake of guests, either in the vapor phase or from aqueous solution, was found to modulate the diffraction efficiency, with the extent of modulation scaling with amount of guest (analyte) taken up as measured independently by quartz crystal microgravimetry [33]. While many of the analytes were sorbed nonspecifically, a few examples of specific binding or molecular recognition were described. Aqueous 2,4,6-tris(4-pyridyl),1,3,5-triazine was sensed with patterned films of **1Zn** but not with films of **1Zn·TPyP** (see Fig. 4 for structure), consistent with uptake based on axial ligation of Zn(II). Molecular square cavity functionalization with tris(aminoethyl)amine yielded films that responded to aqueous  $\text{Zn}^{2+}$ . Functionalization with 1,6-hexanedithiol yielded films responsive to molecular iodine, due to iodine/thiol charge-transfer complex formation.

## 4.3

### Catalysis

Molecular square **1Zn** has been used as an encapsulant for pyridine functionalized manganese porphyrin guests used as catalysts for olefin epoxidation. The protection afforded by guest encapsulation was found to increase the catalyst lifetime by an order of magnitude or more, evidently by inhibiting formation of catalytically inactive oxo-bridged dimers of the manganese porphyrins. The host assembly also engendered substrate size selectivity by preventing access to the active site by large substrate molecules. Modifying the molecular square cavity by ligating pyridine derivatives at two of the

Zn(II) sites, while anchoring the catalyst at the other two, resulted in partial tunability of the substrate size selectivity [34].

#### 4.4

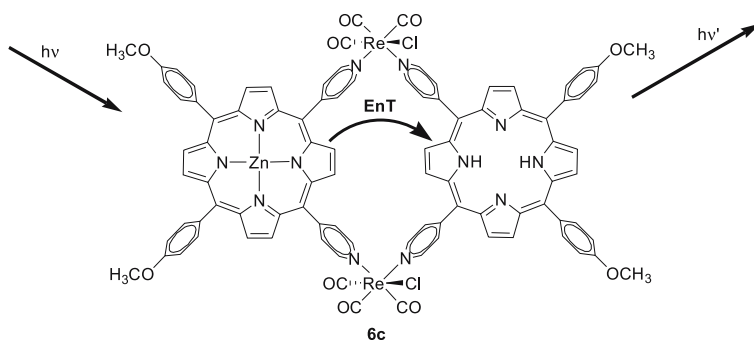
#### Fundamental Studies of Energy and Electron Transfer

Molecular square **1** weakly fluoresces in methylene chloride as solvent [7]. The singlet lifetime is reported to be 2.4 ns. The weak luminescence and relatively short lifetime are presumably consequences of accelerated intersystem crossing caused by proximal heavy atoms (rhenium). When bound as a guest, TPyP is reported to quench  $\sim 90\%$  of the luminescence of **1Zn**. The mechanism of quenching was not established. Excitation of the metallated porphyrins in planar heterodimers **6c** and **7c** was observed to sensitize emission from the free-base porphyrins (Scheme 6) [17]. Energy transfer (EnT) rates of about  $1 \times 10^{10} \text{ s}^{-1}$  were inferred from quantum yields. A factor contributing to efficient transfer may be the porphyrin–porphyrin coplanarity enforced by rhenium coordination. It was argued on energetic grounds that EnT was not mediated by the Re(I) centers.

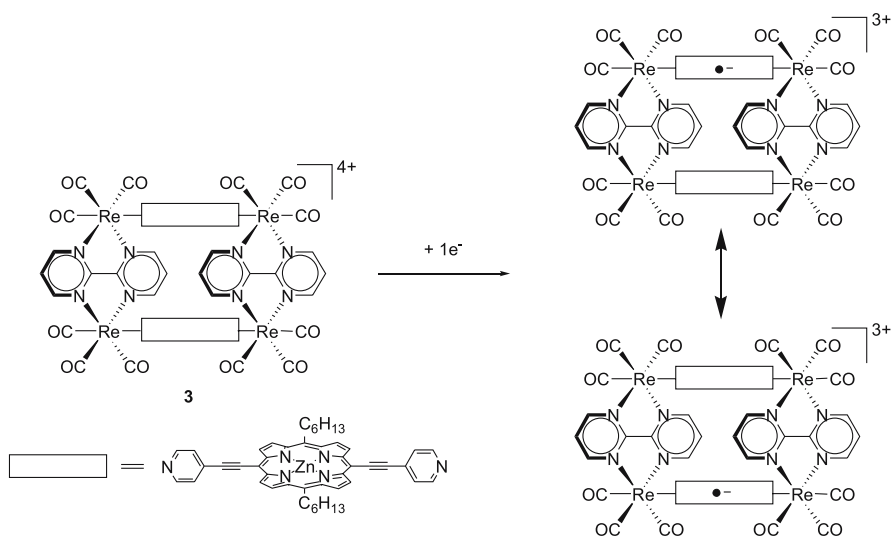
One-electron reduction of the cofacial assembly **4Zn** yields a porphyrin-based mixed-valence compound [35]:

The reduced compound displays an intense intervalence band in the near infrared region. The intervalence transition is nominally a symmetrical charge-transfer transition. Electroabsorbance measurements indicated, however, that only a small amount of charge-transfer character occurs, leading the ground-state form of the assembly to be assigned as a borderline valence-delocalized compound. Electronic structure calculations established that electronic coupling occurs almost entirely by direct donor–orbital/acceptor–orbital overlap. Contributions from superexchange coupling through the rhenium centers were estimated to be less than  $10 \text{ cm}^{-1}$ .

Three-electron reduction also yields a mixed-valence species, but much less strongly electronically coupled as evidenced by the absence of a de-



Scheme 6

**Structure 11**

tectable intervalence absorption band. The reduction in coupling was ascribed to a geometry change: coulombic repulsion between singly and doubly anionic redox centers (i.e., porphyrin ligands) was assumed to yield an open-cavity geometry featuring minimal donor-orbital/acceptor-orbital overlap.

## 4.5

### Light-to-Electrical Energy Conversion

Phosphonated molecular squares have been examined as multilayer sensitizers of indium-tin oxide (conductive glass) surfaces in photoelectrochemical solar cells [36]. Generally, these cells convert energy by the following sequence: (a) dyes are photo-excited, (b) energy is transferred from outer layers to the innermost layer of dye molecules, (c) electrons are transferred from the excited inner layer to the transparent electrode, leaving oxidized dye molecules, (d) dyes are restored to their original form by reduction with a redox shuttle, and (e) the oxidized shuttle molecules diffuse to a dark electrode and are reduced, completing the circuit [37]. Multilayer sensitization typically is only marginally better than monolayer sensitization despite the collection of more photons [38]. One of the problems is believed to be difficulty in moving charge-compensating ions within or through chromophoric layers. In principle, this difficulty could be overcome by using porous molecular square films as light absorbers.

A study done in water as solvent with iodide/triiodide as the redox shuttle exhibited the hoped-for systematic increase in photocurrent with increasing number of dye layers [36]. (Cells with 1 to 15 layers were examined.) The

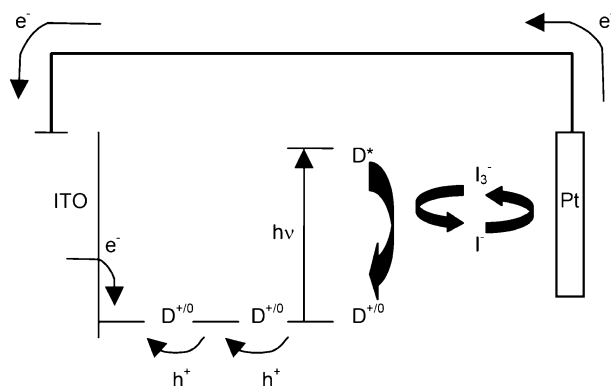


**Fig. 7** Mechanism of cathodic current generation by  $^{13}\text{Zn}$ /ITO multilayer electrodes. Adapted from [36]

direction of current flow, however, was the opposite of what was expected. Further study revealed that the cell operated according to the mechanism shown in Fig. 7. The key feature is direct quenching of the photo-excited porphyrinic square by a pre-associated triiodide ion.

**Acknowledgements** I gratefully acknowledge the contributions of many coworkers whose names are cited in the descriptions of the portions of the reviewed work that were done at Northwestern. I gratefully acknowledge the U.S. Department of Energy, Basic Energy Sciences Offices, for support of our own work on photophysics and energy conversion (grant No. DE-FG87ER13808) and on membranes and molecular sieving (grant No. DE-FG02-01ER15244), and the Northwestern Institute for Environmental Catalysis for support of our work on catalysis.

## References

- Giordano PJ, Wrighton MS (1979) *J Am Chem Soc* 101:2888
- Caspar JV, Sullivan BP, Meyer TJ (1984) *Inorg Chem* 23:2104
- Slone RV, Yoon DI, Calhoun RM, Hupp JT (1995) *J Am Chem Soc* 117:11813
- Fujita M (1998) *Chem Soc Rev* 27:417
- Leininger S, Olenyuk B, Stang PJ (2000) *Chem Rev* 100:853
- Benkstein KD, Hupp JT, Stern CL (2000) *Angew Chem Int Ed* 72:3122
- Slone RV, Hupp JT (1997) *Inorg Chem* 36:5422
- Slone RV, Hupp JT, Stern CL, Albrecht-Schmitt TE (1996) *Inorg Chem* 35:4096
- Lee SJ, Lin W (2002) *J Am Chem Soc* 124:4554
- Sun SS, Lees AJ (2000) *J Am Chem Soc* 122:8956
- Keefe MH, O'Donnell JL, Bailey RC, Nguyen ST, Hupp JT (2003) *Adv Mater* 15:1936
- Miljajac L, Sarkisov L, Ellis DE, Snurr R (2004) *J Chem Phys* 121:7228
- Splan KE, Stern CL, Hupp JT (2004) *Inorg Chim Acta* 357:4005
- Rajendran T, Manimaran B, Liao RT, Lin RJ, Thanasekaran P, Lee GH, Peng SM, Liu YH, Chang IJ, Rajagopal S, Lu KL (2003) *Inorg Chem* 42:6388

15. Thanasekaran P, Liao RT, Liu YH, Rajendran T, Rajagopal S, Lu KL (2005) *Coord Chem Rev* 249:1085
16. Benkstein KD, Stern CL, Splan KE, Johnson RC, Walters KA, Vanhelmont FWM, Hupp JT (2002) *Eur J Inorg Chem* 2002:2818
17. Splan KE, Keefe MH, Massari AM, Walters KA, Hupp JT (2002) *Inorg Chem* 41:619
18. Fan J, Whiteford JA, Olenyuk B, Levin MD, Stang PJ, Fleischer EB (1999) *J Am Chem Soc* 121:2741
19. Iengo E, Milani B, Zangrando E, Geremia S, Alessio E (2000) *Angew Chem Int Ed* 39:1096
20. Santosh G, Ravikanth M (2005) *Inorg Chim Acta* 358:2671
21. Iengo E, Zangrando E, Minatel R, Alessio E (2002) *J Am Chem Soc* 124:1003
22. Williams ME, Hupp JT (2001) *J Phys Chem B* 105:8944
23. Belanger S, Keefe MH, Welch JL, Hupp JT (1999) *Coord Chem Rev* 192:29
24. Massari AM, Gurney RW, Schwartz CP, Nguyen ST, Hupp JT (2004) *Langmuir* 20:4422
25. Kaschak DM, Lean JT, Waraksha CC, Saupe GB, Usami H, Mallouk TE (1999) *J Am Chem Soc* 121:3435
26. Katz HE (1994) *Chem Mater* 6:2227
27. Libera JA, Gurney RW, Nguyen ST, Hupp JT, Liu C, Conley R, Bedzyk MJ (2004) *Langmuir* 20:8022
28. Keefe MH, O'Donnell JL, Bailey RC, Nguyen ST, Hupp JT (2003) *Adv Mater* 15:1936
29. Wamser CC, Bard RR, Senthilathipan V, Anderson VC, Yates JA, Lonsdale HK, Rayfield GW, Friesen DT, Lorenz DA, Stangle GC, Eikren PV, Baer DR, Ransdell RA, Golbeck JH, Babcock WC, Sandberg JJ, Clarke SE (1989) *J Am Chem Soc* 111:8485
30. Czaplewski KF, Hupp JT, Snurr RQ (2001) *Adv Mater* 13:1895
31. Czaplewski KF, Li JL, Hupp JT, Snurr RQ (2003) *J Memb Sci* 221:103
32. Chang SH, Chung KB, Slone RV, Hupp JT (2001) *Synth Met* 117:215
33. Mines GA, Tzeng BC, Stevenson KJ, Li J, Hupp JT (2002) *Angew Chem Int Ed* 41:154
34. Merlau ML, Mejia MDP, Nguyen ST, Hupp JT (2001) *Angew Chem Int Ed* 40:4239
35. Dinolfo PH, Coropceanu V, Bredas JL, Hupp JT, Lee SJ (2005) *Inorg Chem* 44:5789
36. Splan KE, Massari AM, Hupp JT (2004) *J Phys Chem B* 108:4111
37. Hagfeldt A, Grätzel M (2000) *Acc Chem Res* 33:269
38. Taniguchi T, Fukasawa Y, Miyashita T (1999) *J Phys Chem B* 103:1920